Experimental investigation of the occurrence of transonic flow effects on the FFA-W3-211 airfoil

Aditya, Abhyuday; De Tavernier, Delphine; Schrijer, Ferdinand; Van Oudheusden, Bas; Von Terzi, Dominic

DOI
10.1088/1742-6596/2767/2/022031

Publication date
2024

Document Version
Final published version

Published in
Journal of Physics: Conference Series

Experimental investigation of the occurrence of transonic flow effects on the FFA-W3-211 airfoil

Journal of Physics: Conference Series **2767** (2024) 022031 doi:10.1088/1742-6596/2767/2/022031

Experimental investigation of the occurrence of transonic flow effects on the FFA-W3-211 airfoil

Abhyuday Aditya, Delphine De Tavernier, Ferdinand Schrijer, Bas van Oudheusden and Dominic von Terzi

Delft University of Technology, Kluyverweg 1, 2629HS Delft, The Netherlands

E-mail: a.aditya@tudelft.nl

Abstract. For the largest wind turbines currently designed, when operating at rated power and at high wind speeds, the tip airfoils can experience large negative angles of attack. For these conditions and in combination with turbulence, the airfoils are at risk of reaching locally supersonic flow, even at low free-stream Mach numbers. The possibility of shock wave formation and its consequences endangers the lifetime of these largest rotating machines ever built. So far only numerical analyses of this challenge have been attempted with significant modelling uncertainty. Here, for the first time, a wind turbine airfoil (the FFA-W3-211, used at the blade tip of the IEA 15MW reference wind turbine) is studied under transonic conditions using experimental techniques. Schlieren visualization and Particle Image Velocimetry were employed for free-stream Mach numbers of 0.5 and 0.6 and various angles of attack. It was shown that calculations based on isentropic flow theory and compressibility corrections were able to predict the situations where supersonic flow occurred. However, they could not predict the frequency of occurrence and whether shock waves were formed. In conclusion, an unsteady characterization of such airfoil behavior in transonic flow seems to be warranted.

1. Introduction

To meet the ever-increasing global energy demand in a clean and renewable manner, wind turbines have been growing continuously to harness the vast potential of wind power more efficiently and drivers for further growth exist [1]. The next generation of announced offshore wind turbines will have rotor diameters beyond the 240 m of the IEA 15MW reference wind turbine (RWT) [2], and this will give rise to a new set of aerodynamic challenges that have never been encountered before in wind turbine applications. For the IEA 15MW RWT, the design tip speed of the blade is 95 m/s, and combined with a cut-out wind speed of around 25 m/s, the resultant flow experienced by the tip airfoil approaches a Mach number of 0.3. This implies that for larger turbines with higher tip speeds, the common design assumption of incompressible flow may no longer be valid.

Flow compressibility brings with it the risk of undesirable phenomena such as shock waves. Only a few studies have focused on the possible occurrence of such high-speed flow features in wind turbine applications: Wood [3] studied small horizontal axis wind turbines with NACA0012 airfoils and high tip-speed ratio to explore the possibility of using shock-induced separation at the tips as a means of overspeed protection, but symmetric airfoils are not used at utility-scale wind turbine blade tips. Hossain et al. [4] investigated the propagation of shock waves on an NREL Phase VI S809 wind turbine airfoil using 2D RANS with increasing angles of attack.

However, the study was conducted at a free-stream Mach number of 0.8, which, at the moment, is understood to be far too high to be of relevance for current wind turbine applications.

The occurrence of supersonic flow features corresponding to real-world conditions of large wind turbines has not been investigated extensively yet, as only recently wind turbines have grown large enough to experience tip speeds near Mach 0.3. For offshore deployment of large wind turbines, dynamic effects such as free-stream turbulence, the aeroelastic response of the blade, and the floating motion of offshore structures may contribute to a further increase of the (instantaneous) wind speed experienced by the tip airfoil. Moreover, during operation at rated power close to cut-out conditions, the tip airfoils are exposed to large negative angles of attack (AoAs). The investigation of De Tavernier and von Terzi [5] revealed and [6] corroborated with RANS simulations that, for the IEA 15MW RWT, at such conditions, combined with inflow turbulence, the resulting strong suction peak may push the tip airfoil into a transonic flow regime. This may result in the formation of shock waves at the blade tip, which is undesirable as it leads to a loss in performance. Furthermore, the presence of shocks may lead to flow unsteadiness in the location of the shock as well as separation features, typically referred to as transonic buffeting (already studied extensively for supercritical airfoils [7]), which can cause strong vibrations with a high risk of significantly reducing the lifetime of wind turbine blades.

While compressibility effects on wind turbine performance have been investigated previously using numerical simulations as in [6] and references therein, to our knowledge, there exist no reliable measurements of typical wind turbine airfoils operating in the compressible flow regime. Hence, there is an urgent need to understand the conditions under which supersonic flow occurs over typical wind turbine airfoils and whether this will lead to the formation of shocks. The current study focuses on the FFA-W3-211 airfoil, which is used as the tip airfoil on the IEA 15MW wind turbine. Experimental techniques are employed to characterize the flow physics of the airfoil under transonic flow conditions.

2. Methodology

2.1. Wind tunnel facility

Measurements on a static FFA-W3-211 airfoil are performed in the TST-27 transonic-supersonic blowdown-type wind tunnel at the Delft University of Technology (Figure 1). The free-stream Mach number in the test section is controlled by a choke mechanism downstream of it. The test section is 255 mm $\times$ 280 mm in height and width, respectively, with optical access from both side walls. The total pressure is set to $p_0 = 2$ bar in the current experiments, while the total temperature is $T_0 = 288$ K. The Mach number in the transonic range can be varied from 0.5 ± 0.01 to 0.85 ± 0.01. For the current study, Mach numbers of 0.5 ± 0.01 and 0.6 ± 0.01 are used, which corresponds to free-stream velocities of 166 and 197 m/s.

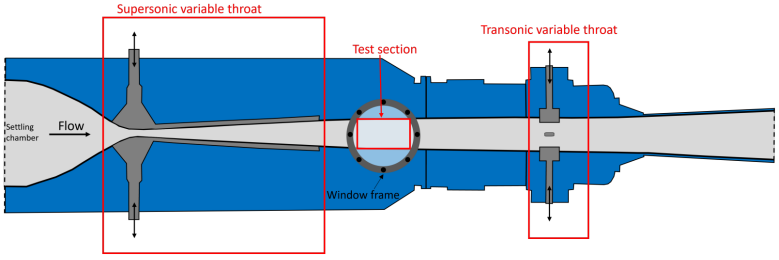

Figure 1: A schematic of the Transonic-Supersonic wind tunnel (TST-27) [9].

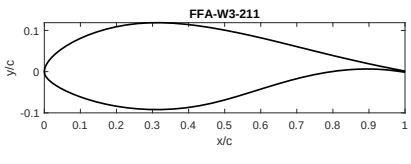

Figure 2: The FFA-W3-211 airfoil.

2.2. Wind tunnel model

The tip airfoil used in the IEA 15MW RWT is the FFA-W3-211 (see Figure 2), belonging to the DTU FFA series [8]. A model of the airfoil with a chord of 70 mm was used for the tests. The model spans the entire width of the test section, resulting in an aspect ratio of 4. While testing in the wind tunnel, the airfoil model is installed upside-down compared to the conventional orientation shown in Figure 2. This is because the lower side of the airfoil will act as the suction side at negative AoAs, which are of primary interest in the current study, as explained in Section 3.1. The AoA of the model is set manually using a digital angle gauge with an accuracy of 0.1°, and the values reported throughout refer to the geometric AoA, which would be different from the actual AoA in the test section due to wall interference effects on the streamline curvature.

2.3. Schlieren

Schlieren maps the gradient of the refractivity of a medium, which can be interpreted as a visualization of gradients of density and is thus useful for identifying compressible flow features such as shock and expansion waves. However, no 3D or quantitative information can be derived from the conventional Schlieren technique. For the current study, a Z-type Schlieren setup is employed, using a white LED for illumination, and images are acquired at 100 Hz using a LaVision Imager sCMOS at a resolution of 1920 × 1038 pixels, corresponding to a field of view of 112 mm × 61 mm in streamwise and vertical extent.

2.4. Particle Image Velocimetry

Particle Image Velocimetry (PIV) is used in planar configuration to measure the velocity field at the spanwise center of the airfoil model. For illumination a Nd:YAG laser is used, operated at a repetition rate of 15 Hz. A LaVision Imager sCMOS camera is used to acquire the particle images, spanning a field of view of 52 mm × 44 mm in the streamwise and vertical directions, respectively, at a scale of approximately 49 px/mm. After processing the raw images to obtain the velocity field, there are 6.1 vectors per mm in physical space, in both streamwise and vertical directions. A schematic of the setup along with the field-of-view for different cases is presented in Figure 3.

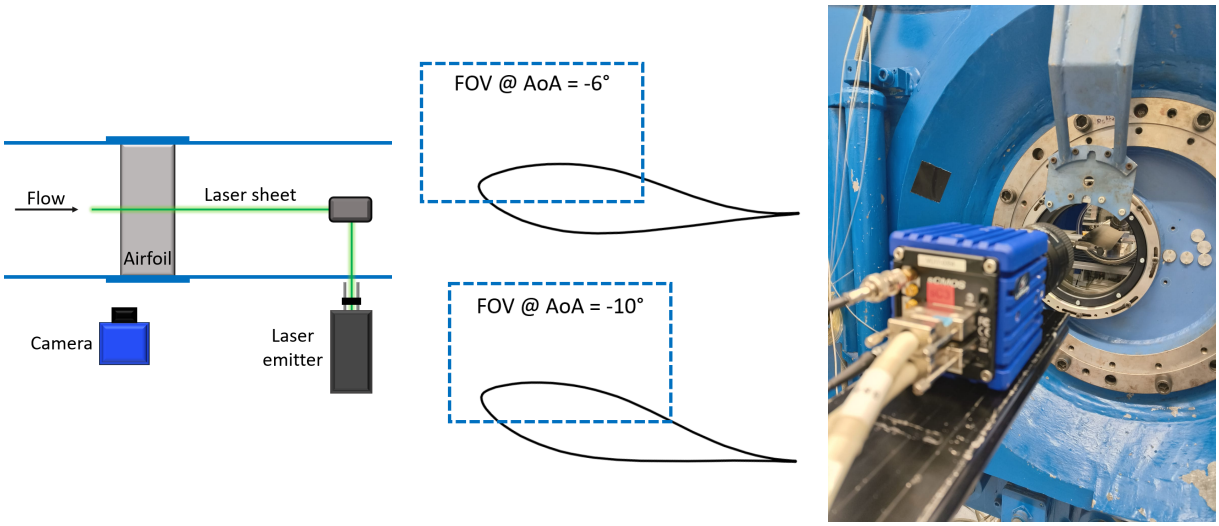

Figure 3: PIV setup details, showing the camera and laser arrangement around the test section on the left, the fields-of-view in the middle, and a view of the camera and test section on the right.

3. Results

3.1. Transonic envelope and experimental design

In their study, De Tavernier and von Terzi [5] calculated the envelope separating the subsonic regime and (local) supersonic flow regime in terms of the critical pressure coefficient, $C_{p,cr}$, and the free-stream Mach number, Ma_∞, employing isentropic compressible flow theory (Prandtl-Glauert correction). Using RFoil simulations, this was translated in terms of Ma_∞ and the AoA for the FFA-W3-211 by determining at which AoA the $C_{p,cr}$ was first reached for a given Ma_∞, see Figure 4. With the help of this envelope, simulations in OpenFAST revealed that the IEA 15MW RWT when operating near cut-off wind conditions at high free-stream turbulence levels may encounter large negative angles of attack (in the order of $-10°$ to $-15°$) at the blade airfoils. Some of these operating points could then possibly experience local regions of supersonic flow. The same supersonic envelope calculations are used to inform the experimental design of the current study. The blade tip of the IEA 15MW RWT reaches maximum relative wind speeds of less than Mach 0.3 when the flow becomes locally supersonic (as shown by the blue points farthest to the left in Figure 4).

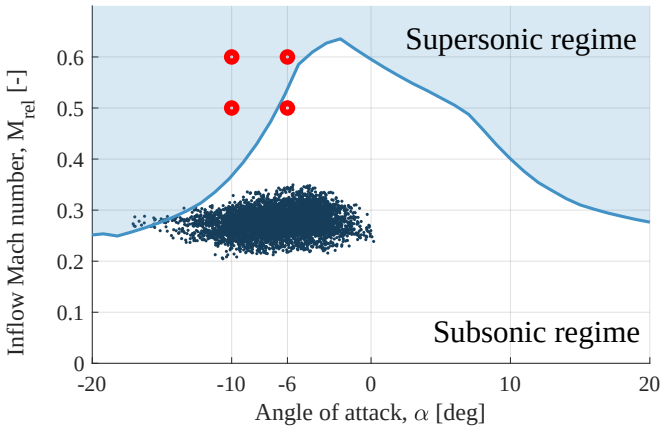

Figure 4: The supersonic envelope for FFA-W3-211 derived by De Tavernier and von Terzi (2022). The blue points represent conditions at the tip of the blade of the IEA 15MW RWT as revealed by OpenFAST simulations. Marked in red are the experimental test conditions for the current study.

Table 1: Free-stream Mach numbers and corresponding Reynolds numbers.

Ma_∞	Re_c
0.5	1.4×10^6
0.6	1.6×10^6

The test conditions for conducting experiments are limited by the capabilities of the choke mechanism of the wind tunnel, which currently allows only for a minimum Ma_∞ of 0.5 in the test section. Two test points were chosen, at AoAs of $-6°$ and $-10°$, for both $Ma_\infty = 0.5$ and $Ma_\infty = 0.6$. As mentioned before, the geometric AoAs are reported here, without corrections for streamline curvature due to wall interference. Also, Ma_∞ is not corrected for blockage effects. This choice of Ma_∞ and AoAs combinations allows for studying a transition from a complete subsonic regime to a local supersonic regime, through both an increase in the (negative) AoA, representing increased geometrical curvature for the same free-stream conditions, as well as an increase in free-stream Mach number for the same geometry (i.e., AoA). Also, all results presented henceforth will show the airfoil in an inverted position, as explained previously (compare Figure 3).

The free-stream Mach number is set by the wind tunnel control system and is used to calculate the free-stream velocity, which in turn is used to determine the chord-based free-stream Reynolds number, Re_c, as follows:

$$Ma_\infty = \frac{U_\infty}{\sqrt{\gamma R T_\infty}}, \; Re_c = \frac{\rho_\infty U_\infty c}{\mu_\infty}$$

where T_∞ is determined from the total temperature, T_0, and Ma_∞. The free-stream density, ρ_∞, is calculated from the total pressure (p_0), as measured in the wind tunnel settling chamber, using the isentropic relations and the perfect gas equation for air. The free-stream dynamic viscosity is extracted from Sutherland's law, for the given T_∞. For the current test conditions, $p_0 = 2$ bar and $T_0 = 288$ K, the Re_c obtained are presented in Table 1.

3.2. Local Mach number trends

Using the energy equation for isentropic flow, the local Mach number can be related to the local velocity magnitude, U, and the total temperature of the flow, T_0:

$$Ma = \frac{U}{\sqrt{\gamma R T_0 - \left(\frac{\gamma-1}{2}\right) U^2}}$$

The total temperature is measured in the settling chamber of the TST-27 (see Figure 1), using a thermocouple with an accuracy of ± 1°C. During the experiments, the measured total temperature varied in the range 15-17°C. The overall results were not found to be remarkably sensitive for different total temperatures in the given range, hence, an average value of $T_0 = 288$ K is used throughout. Since both streamwise and vertical velocity components are obtained from the post-processed PIV measurements, it is relatively straightforward to determine the local Mach numbers using the aforementioned formula. In all figures presented henceforth, the flow direction is from left to right.

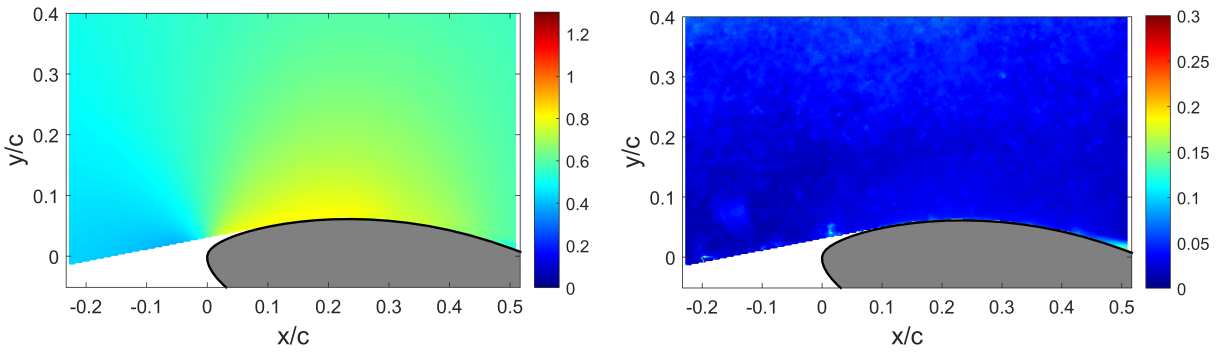

(a) Mean (b) Standard deviation

Figure 5: Contours of Mach number: (a) mean value and (b) standard deviation; $Ma_\infty = 0.5$, AoA $= -6°$.

The mean and standard deviation of the local Mach numbers for the fully subsonic case, with $Ma_\infty = 0.5$ and AoA $= -6°$, as predicted by Figure 4, is presented in Figure 5a and Figure 5b, respectively. The maximum mean local Mach number slightly exceeds 0.8 for this configuration, as seen in Figure 5a, and from the contours it is seen that the flow smoothly accelerates over the airfoil from its free-stream conditions, without shock waves or separation. In the region where the mean Mach number is maximum (> 0.8), $x/c \approx 0.1 - 0.25$, the standard deviation is only about 0.05 (see Figure 5b), and thus it is clear that sonic conditions are not achieved for the given configuration.

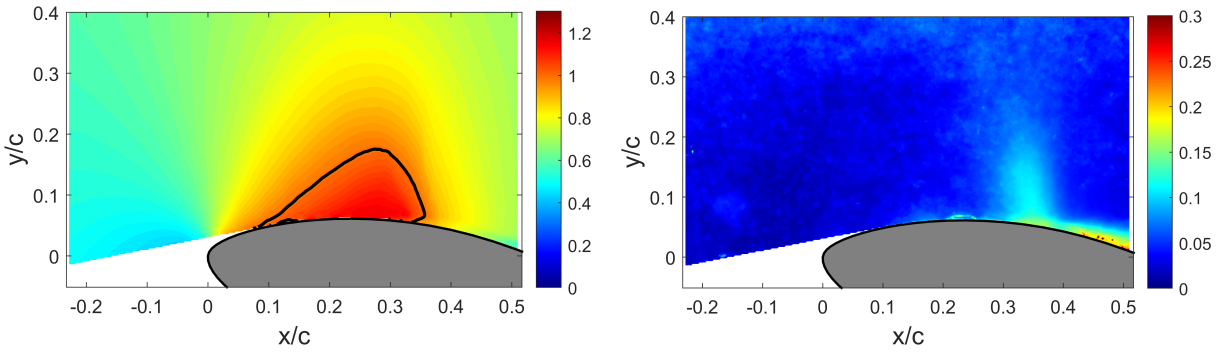

(a) Mean (b) Standard deviation

Figure 6: Contours of Mach number: (a) mean value and (b) standard deviation; $Ma_\infty = 0.6$, AoA $= -6°$. The solid black line represents a local Mach number of 1.

Upon increasing the Mach number to 0.6 in the free-stream while keeping the same AoA of $-6°$, the flowfield changes significantly. Now, the mean flow becomes supersonic, as seen in Figure 6a, where a local Mach number equaling unity (sonic conditions) is marked with a solid black line, which extends from 5-35% of the chord in the streamwise direction close to the airfoil. The region enclosed by this sonic line is supersonic in terms of the mean flow. Looking at the standard deviation for the same configuration, presented in Figure 6b, there seem to be significant fluctuations in the Mach number, varying in the range $\approx 0.1 - 0.15$, between $x/c = 0.3$ and $x/c = 0.4$. For the same streamwise extent, the mean Mach number varies in the range $\approx 0.9 - 1.1$ (Figure 6a), which indicates that the region may experience both subsonic and supersonic flow intermittently. This may also suggest the presence of an oscillating shock wave over the same region, but it is not clear from just the mean and standard deviation contours and will be investigated further in Section 3.4. There is a suggestion of a shallow, unsteady separation of the shear layer, for a thin region extending downstream from $x/c = 0.4$.

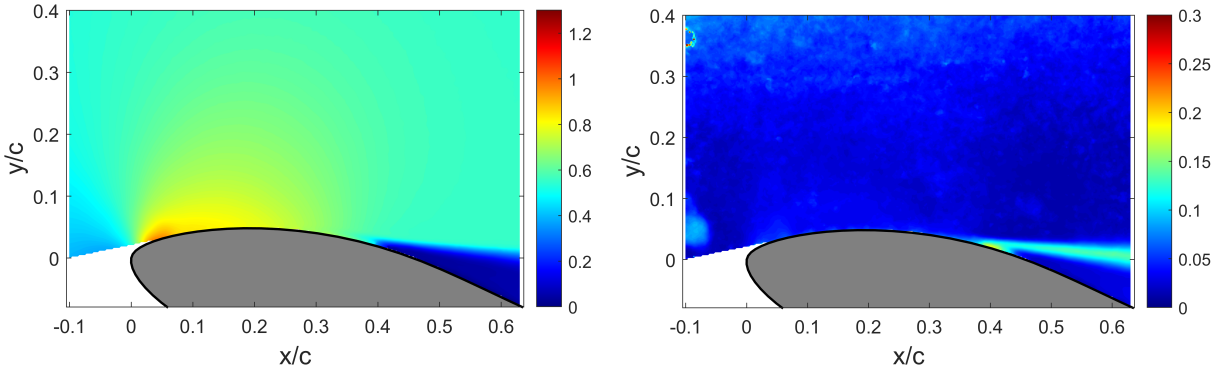

(a) Mean (b) Standard deviation

Figure 7: Contours of Mach number: (a) mean value and (b) standard deviation; $Ma_\infty = 0.5$, AoA $= -10°$.

Now, for the lower free-stream Mach number of 0.5 and the steeper AoA of $-10°$, the calculations of De Tavernier and von Terzi [5] indicate that supersonic flow is expected, as seen in Figure 4. The experimental results of the mean flow for $Ma_\infty = 0.5$, AoA $= -10°$ are presented in Figure 7a, and the maximum local Mach number is found to be barely reaching a local Mach number of 1 very close to the leading edge (between $x/c = 0$ to 0.1). However, the

standard deviation of the Mach number in the same region, see Figure 7b, is at maximum 0.1, which could be an indication of the flow becoming locally supersonic in an intermittent sense but not consistently enough for a supersonic mean flow to be observed. This is further addressed in Section 3.3.

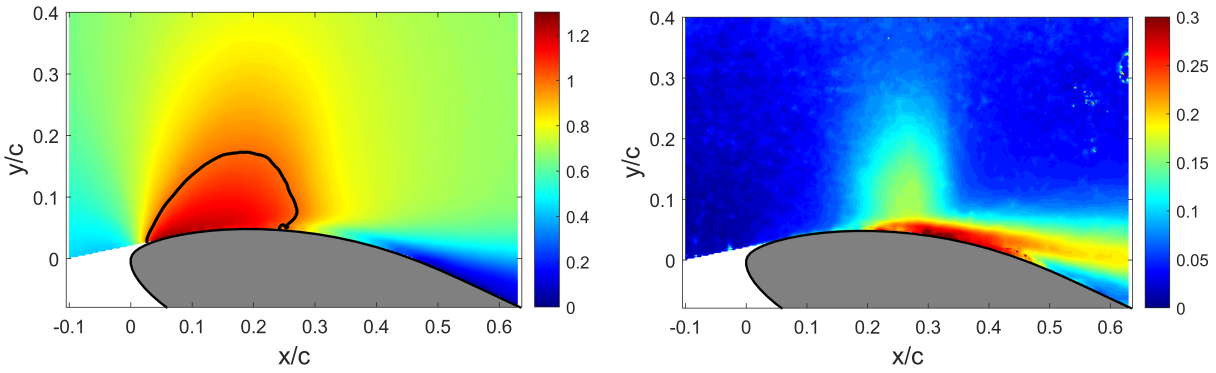

(a) Mean (b) Standard deviation

Figure 8: Contours of Mach number: (a) mean value and (b) standard deviation; $Ma_\infty = 0.6$, AoA $= -10°$. The solid black line represents a local Mach number of 1.

Finally, in the most drastic case with $Ma_\infty = 0.6$, AoA $= -10°$, supersonic flow is again obtained in the mean sense as shown in Figure 8a, with the sonic line (indicated in black) extending to $x/c \approx 0.3$. The sonic line in this case is seen to be more upstream compared to the case of $Ma_\infty = 0.6$, AoA $= -6°$ (in Figure 6a), which is explained by the steeper AoA resulting in a stronger suction peak and faster acceleration of the flow near the leading edge.

In Figure 8b, a vertical region of high standard deviation exists between $x/c \approx 0.15 - 0.35$ up to $y/c \approx 0.2$ from the airfoil surface, where the standard deviation in the local Mach number reaches 0.15. With the mean Mach number in the same region being around 0.9-1.2, this may be an indication of a moving shock wave (with the instantaneous Mach number varying between 0.75-1.35); this is investigated further in subsection 3.4 by examining instantaneous Mach number contours. This region is qualitatively similar to the case of $Ma_\infty = 0.6$, AoA $= -6°$ as shown in Figure 6b, albeit the latter is observed to be more downstream as a result of the shallower AoA which would cause the shock to occur farther downstream.

Furthermore, an elevated standard deviation in local Mach number, ranging from 0.2-0.3, is observed close to the airfoil starting from $x/c = 0.2$ and extending downstream beyond the end of the FOV (see Figure 8b). This suggests the presence of a fluctuating shear layer, involving the interaction between the separated boundary layer and the unsteady shock wave. Interestingly, no such region was observed for $Ma_\infty = 0.6$, AoA $= -6°$ (Figure 6b), which suggests that in that case, shock-induced separation might be relatively weaker, if at all present. On the other hand, a similar separated shear layer signature can be observed for $Ma_\infty = 0.5$, AoA $= -10°$ (Figure 7b), but with a much lower level of unsteadiness.

It is worth mentioning that in the present data, no outlier removal was performed for any of the cases here presented, which explains the occurrence of relatively high standard deviation values in some free-stream regions near the edges of the field-of-view, due to erratic seeding in the PIV measurements. However, for this study, only the region near the airfoil is focused on, where the results show a close correspondence with expected flow physics.

3.3. Probability of supersonic flow

While the mean flow for $Ma_\infty = 0.5$, AoA$=-10°$ barely reaches supersonic values, it is also important to know if the flow might be occasionally supersonic, in an intermittent sense. To

investigate this, the local Mach numbers are calculated for all the recorded PIV frames separately. Any vector going supersonic is identified and recorded. From the number of occurrences of supersonic flow at a particular location, the probability of obtaining supersonic flow there is calculated by simply dividing by the total number of recorded frames.

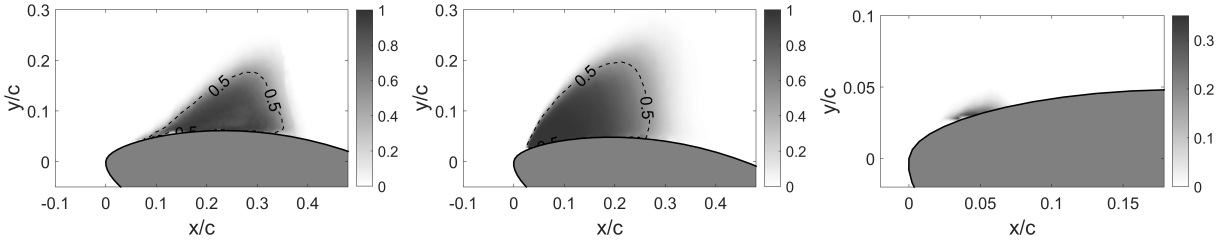

(a) $Ma_\infty = 0.6$, AoA$=-6°$ (b) $Ma_\infty = 0.6$, AoA$=-10°$ (c) $Ma_\infty = 0.5$, AoA$=-10°$

Figure 9: Probability of supersonic flow mapped for different cases. The contour corresponding to 0.5 is marked with a dashed line in (a) and (b). Note that the magnification and the contour scale are different for (c).

The probability maps obtained for the higher free-stream Mach number of 0.6 are presented for AoA$=-6°$ (Figure 9a) and AoA$=-10°$ (Figure 9b), and both demonstrate similar characteristics in a qualitative sense. The region enclosing a minimum chance of 50% for the occurrence of supersonic flow is flatter (maximum $y/c \approx 0.18$) and more elongated (x/c ranging from 0.05 to 0.35) for AoA$=-6°$ as compared to AoA$=-10°$, where the same 50% probability of supersonic flow occurs over $y/c \approx 0.2$ and $x/c \approx 0.02 - 0.25$, i.e. farther upstream, as expected with a steeper AoA. Supersonic flow appears more frequently within the region enclosed by the contour corresponding to 50% probability of supersonic flow, as seen in Figure 9a and Figure 9b. It makes sense that we see such high probabilities of supersonic flow since the mean flow also exhibits a significant region of local Mach numbers beyond 1 in both cases, as seen in Figure 6a and Figure 8a.

Finally, in the probability map corresponding to the lower Mach number of 0.5 and at an AoA of $-10°$, as shown in Figure 9c, we observe that only a very small region near the airfoil leading edge, barely 5% of the chord in extent, appears to experience supersonic flow, in 10-35% of the total frames. Thus, the flow speeds breach local sonic conditions in an intermittent sense and only in a very small and flat region. Also, likely, the pressure gradient is not strong enough to result in a flow acceleration sufficient for creating shock waves, and the flow might decelerate smoothly to subsonic conditions. Note that the scale extends to a maximum probability of only 0.35 in this case (Figure 9c), compared to a maximum of 1 in the previous cases (Figure 9a and Figure 9b). It is evident that a drop in Ma_∞ from 0.6 to 0.5 drastically alters the flow behaviour for the same AoA of $-10°$, despite both conditions lying deep inside the predicted supersonic regime according to the supersonic envelope calculations shown in Figure 4.

3.4. Appearance of shock waves

Instantaneous Schlieren images provide a clear visualization of density gradients in the flow and, hence, allow to detect the occurrence of shock waves. In the current Schlieren images, compression regions such as shock waves, appear darker than the gray background.

In the case of $Ma_\infty = 0.5$, AoA$=-10°$, no strong shock waves can be discerned at the top of the airfoil in Figure 10, as expected from the previous results. In contrast, a group of shock waves can be clearly distinguished for the same AoA at $Ma_\infty = 0.6$ in Figure 11. Multiple shocks are seen because the wind tunnel sidewalls result in a spanwise distribution of the shock

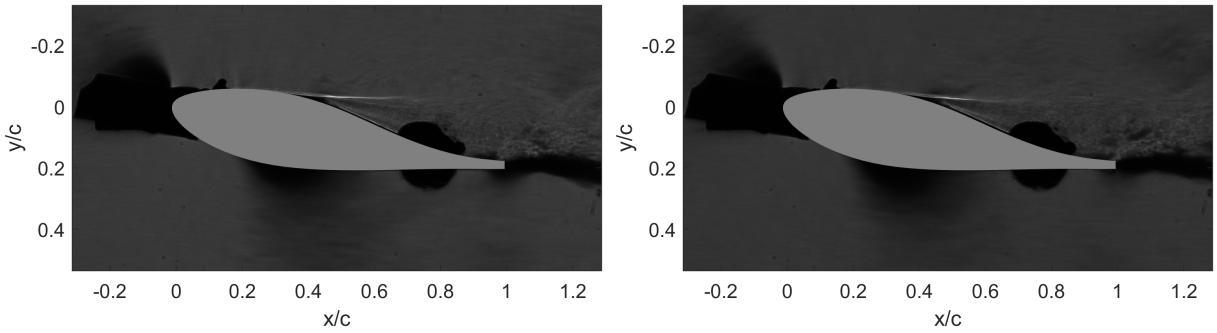

Figure 10: Instantaneous Schlieren images for $Ma_\infty = 0.5$, AoA=$-10°$. No shock waves can be discerned at the top of the airfoil.

front, and Schlieren is unable to isolate a single plane. It is, therefore, unclear how exactly the shock wave is distributed along the spanwise direction in Figure 11.

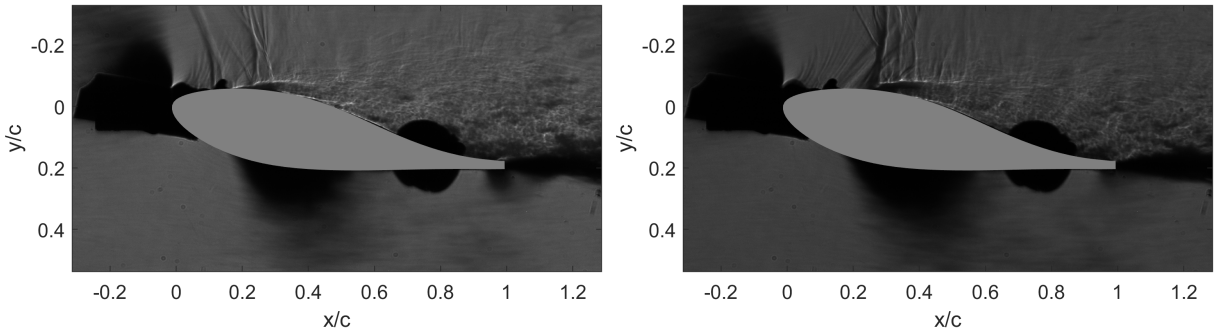

Figure 11: Instantaneous Schlieren images for $Ma_\infty = 0.6$, AoA=$-10°$ showing the appearance of a shock wave.

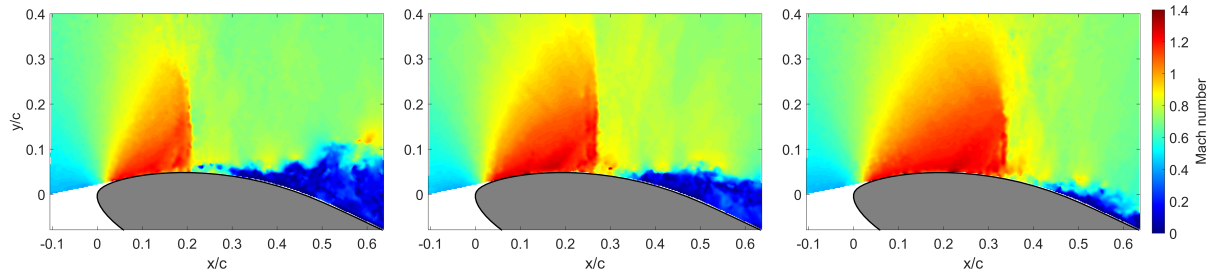

Figure 12: Instantaneous frames for $Ma_\infty = 0.6$, AoA=$-10°$ showing the appearance of a moving shock wave at different streamwise locations over the airfoil.

With PIV, the shock waves are identified more unambiguously since the measurements correspond to a single plane, which is at the spanwise center of the model in this case. At an AoA of $-10°$ and $Ma_\infty = 0.6$, the shock wave also demonstrates an unsteady nature, as seen from instantaneous Mach number contours shown in Figure 12. The shock is observed to vary between $x/c = 0.2$ in the leftmost frame to $x/c = 0.35$ in the rightmost frame. These locations are in good agreement with the region of high standard deviation in the local Mach number ($x/c = 0.15 - 0.35$) identified as an outcome of the shock motion in Figure 8b. However,

the acquisition frequency of the PIV measurements is not sufficient to calculate characteristic frequencies of the shock movement. Furthermore, the different flow field snapshots Figure 12 give further evidence of a high unsteadiness of the separated flow region, which appears to be related with the shock motion.

4. Discussion

For the higher Ma_∞ of 0.6, shock waves were experimentally confirmed to occur at both AoAs ($-6°$ and $-10°$), with both conditions predicted to exhibit supersonic flow according to Figure 4. This was reflected in the mean and standard deviation of the local Mach number, with the former highlighting large regions of supersonic flow, and the latter identifying the existence of unsteady shock waves. When Ma_∞ was lowered to 0.5 for an AoA of $-10°$, that was predicted to be well within the supersonic flow regime in Figure 4, no shock waves were observed. A considerably smaller region with an extent of 5% of the chord was seen to experience supersonic flow intermittently, in a maximum of around 1/3 of the total frames. In the other two cases, supersonic flow occurred more consistently over a significantly greater extent (see Figure 9a and Figure 9b). Note, that with the Mach number also the Reynolds number slightly changed.

Likely, for $Ma_\infty = 0.5$, the suction peak was not strong enough to cause a sufficient flow acceleration to produce larger regions of supersonic flow and eventually shock waves. This could be due to an effective de-cambering of the airfoil at the given AoA of $-10°$ following a large separation of the boundary layer. However, this de-cambering effect is not seen to be equally effective, despite increased separation, when the free-stream Mach number is raised to 0.6 for the same AoA of $-10°$. Thus, the calculation of the supersonic envelope presented in Figure 4 is not sufficient to predict the occurrence of shock waves.

5. Conclusions

As presented in Figure 4, basic calculations using isentropic flow theory and compressibility corrections, combined with low-fidelity airfoil design tools such as RFoil allow to predict the combinations of free-stream Mach number and AoA to obtain supersonic flow over the FFA-W3-211. While these calculations tell us when to expect supersonic flow or not, they cannot predict the frequency and intensity of the supersonic flow features. Moreover, the current study shows that there may exist a substantial disparity in flow features for conditions that are predicted to lie deep inside the supersonic regime, warranting a more comprehensive and unsteady characterization of such airfoil behavior in transonic flow conditions.

The primary limitation of this study is that the Mach number range studied here is beyond the expected operational range of large wind turbines at present. It is possible that at conditions closer to $Ma_\infty = 0.3$ and AoA of $-15°$, where the IEA 15 MW blade tip is predicted to experience the supersonic regime in Figure 4, the flow physics might turn out to be surprisingly different!

References

[1] Mehta M, Zaiijer M, von Terzi D 2024 Drivers for optimum sizing of wind turbines for offshore wind farms *Wind Energ. Sci.* **9** 141–163
[2] Gaertner E, Rinker J, Sethuraman L, Zahle F, Anderson B, Barter G, Abbas N, Meng F, Bortolotti P, Skrzypinski W, Scott G, Feil R, Bredmose H, Dykes K, Shields M, Allen C and Viselli A 2020 Definition of the IEA wind 15-megawatt offshore reference wind turbine Report NREL/TP-5000-75698 National Renewable Energy Laboratory
[3] Wood D H 1997 Some effect of compressibility on small horizontal-axis wind turbines *Renewable Energy* **10** 11–17
[4] Hossain M A, Huque Z and Kammalapati R R 2013 Propagation of shock on NREL phase VI wind turbine airfoil under compressible flow *Journal of Renewable Energy* **2013** 653103
[5] De Tavernier D and von Terzi D 2022 The emergence of supersonic flow on wind turbines *Journal of Physics: Conf. Series* **2265** 042068

[6] Vitulano M C, De Tavernier D, de Stefano G and von Terzi D 2024 Numerical analysis of static and dynamic wind turbine airfoil characteristics in transonic flow *Journal of Physics: Conf. Series*
[7] D'Aguanno A, Schrijer F F J and van Oudheusden B W 2021 Experimental investigation of the transonic buffet cycle on a supercritical airfoil *Experiments in Fluids* **62** 214
[8] Bertagnolio F, Sørenson N N, Johansen J and Fuglsang P 2001 *Wind turbine airfoil catalogue*
[9] D'Aguanno A 2023 *Physics and control of transonic buffet* PhD thesis Delft University of Technology